Accepted Manuscript

Real-time monitoring of magnetic drug targeting using fibered confocal fluorescence microscopy

Jie Bai, Julie Tzu-Wen Wang, Kuo-Ching Mei, Wafa T. Al-Jamal, Khuloud T. Al-Jamal

Real-Time Monitoring of Magnetic Drug Targeting Using Fibered Confocal Fluorescence Microscopy

Jie Bai[1][†], Julie Tzu-Wen Wang[1][†], Kuo-Ching Mei[1], Wafa T. Al-Jamal[2], Khuloud T. Al-Jamal[1]*

[1]Institute of Pharmaceutical Science, Faculty of Life Sciences & Medicine
King's College London, SE1 9NH (UK)

[2]School of Pharmacy, University of East Anglia, Norwich Research Park, Norwich NR4 7TJ, UK

* Corresponding-Author
Dr Khuloud T. Al-Jamal
Institute of Pharmaceutical Science, Faculty of Life Sciences & Medicine
King's College London, SE1 9NH (UK)
E-mail: khuloud.al-jamal@kcl.ac.uk

[†] Contributed equally to the work

Abstract

Magnetic drug targeting has been proposed as means of concentrating therapeutic agents at a target site and the success of this approach has been demonstrated in a number of studies. However, the behavior of magnetic carriers in blood vessels and tumor microcirculation still remains unclear. In this work, we utilized polymeric magnetic nanocapsules (*m*-NCs) for magnetic targeting in tumors and dynamically visualized them within blood vessels and tumor tissues before, during and after magnetic field exposure using fibered confocal fluorescence microscopy (FCFM). Our results suggested that the distribution of *m*-NCs within tumor vasculature changed dramatically, but in a reversible way, upon application and removal of a magnetic field. The *m*-NCs were concentrated and stayed as clusters near a blood vessel wall when tumors were exposed to a magnetic field but without rupturing the blood vessel. The obtained FCFM images provided *in vivo in situ* microvascular observations of *m*-NCs upon magnetic targeting with high spatial resolution but minimally invasive

1

surgical procedures. This proof-of-concept descriptive study in mice is envisaged to track and

quantify nanoparticles *in vivo* in a non-invasive manner at microscopic resolution.

1. Introduction

Magnetic drug targeting has been shown to be a promising method of concentrating therapeutic agents at a target site, and allowing higher drug doses to be administered while still being tolerated by patients .[1-3] A number of studies have demonstrated that magnetic nanoparticles (MNPs) can be magnetically targeted to tumor sites and the targeting effect has been assessed by various techniques, including optical imaging, magnetic resonance imaging (MRI) and histology studies (Prussian blue staining).[4-11] These studies have suggested that a higher concentration of magnetic therapeutic agents can be achieved upon the application of an external magnetic field. However, the magnetic behaviors of MNPs in blood vessels and tumor microcirculation have not been demonstrated. The previously employed imaging methods cannot offer sufficient resolution to show how MNPs travel through blood vessels and accumulate in tumors, whereas histological studies can only provide *ex vivo* information at post-mortem in a non-dynamic way. Some studies have been carried out using *ex vivo* artery models or mathematical simulation to characterize the MNPs behaviors in blood vessels and/or surrounding tissues, but no *in vivo* studies have been performed so far.[12-15] Here we visualized the magnetic capture of *m*-NCs within blood vessels and tumor tissues in real-time *in vivo* before, during and after magnetic field exposure. The magnetic targeting efficacy of *m*-NCs was firstly quantified by gamma counting and this was further confirmed by direct imaging of the magnetic targeting process in blood vessel on the microscopic scale. This proof-of-concept descriptive study in mice is envisaged to track and quantify nanoparticles *in vivo* in a non-invasive manner with microscopic resolution.

2. Material and methods

2.1 Material

3

'Ferrofluid' magnetic oil (oleic acid coated SPIONs with diameter of 10 nm, suspended in kerosene at 10^{17} particles per ml) was purchased from Magnacol Ltd (UK). Soybean lecithin (Epikuron 140 V) was a kind gift from Cargill Pharmaceuticals (USA). Polyoxyethylene-bis-amine (NH_2-$PEG_{3.5kDa}$-NH_2) was purchased from JENKEM (USA). D/L-lactide/glycolide copolymer 75/25 ($PLGA_{18kDa}$-COOH) was purchased from Purac Biomaterials (the Netherlands). Tween® 80, nitric acid, methanol, dimethylsulphoxide (DMSO) and dichloromethane were obtained from Fisher Scientific Ltd (UK). Fluorescein isothiocyanate–dextran (FITC-Dextran, average molecular weight 2,000 kDa), sodium chloride, diethylene triamine pentaacetic acid (DTPA), castor oil, ethylenediaminetetraacetic acid disodium salt dehydrate (EDTA) and Sephadex® G-75 were purchased from Sigma Aldrich (UK). 1,1-dioctadecyltetramethyl indotricarbocyanine Iodide (DiR) was obtained from Cambridge Bioscience (UK). Advanced RPMI-1640 media, penicillin-streptomycin 100X, 0.25 % Trypsin-EDTA with phenol red, Glutamax™ supplement, phosphate buffered saline PBS (10X, pH 7.4) and phosphate buffered saline PBS (1X, pH 7.4) were obtained from Gibco, Invitrogen (UK). Fetal bovine serum (FBS) was obtained from First-Link Ltd (UK). Pentobarbital sodium (Euthatal®) was obtained from Merial (UK). PD-10 desalting column was obtained from GE Healthcare Life Sciences (UK).

2.2 Preparation and characterization of *m*-NCs and *m*-NC-DiR

The magnetic polymeric nanocapsules (*m*-NCs) were prepared by single emulsification/solvent evaporation method.[1] $PLGA_{18kDa}$-$PEG_{3.5kDa}$-NH_2 and $PLGA_{18kDa}$-$PEG_{3.5kDa}$-DTPA were synthesized as described in our previous work.[16, 17] Briefly, $PLGA_{18kDa}$-$PEG_{3.5kDa}$-NH_2 (12.5 mg, 10% w/w $PLGA_{18kDa}$-$PEG_{3.5kDa}$-DTPA was incorporated for *m*-NCs to be used for radiolabeling), castor oil (75 mg), soybean lecithin (25 mg) and increasing amounts of SPIONs (0, 0.5, 2.5 or 10 mg) were dissolved in 2.5 ml dichloromethane. DiR was incorporated into *m*-NCs formulation at 0.5% w/w DiR/castor oil

for fibered confocal fluorescence microscopic (FCFM) imaging. The organic phase was poured into an aqueous phase (5 ml) containing Tween® 80 (20 mg) as a hydrophilic surfactant. The resultant dispersion was emulsified by ultra-sonication using a probe sonicator (Soniprep 150, UK) at 15 micro amplitude for 180 s in an ice bath. Organic solvents were then evaporated in a chemical fume hood for 20 min. The final volume of the *m*-NC suspension was adjusted to 5 ml. The obtained *m*-NC suspension was further condensed by 10 (FCFM imaging) or 20 times (gamma counting), with rotary evaporator, yielding 25 and 50 mg/ml of polymer, respectively.

2.3 Size and zeta potential measurements

The hydrodynamic size (Z-Average), polydispersity index (PDI) and zeta potential of NCs and *m*-NCs were determined by NanoZS (Malvern Instrument, UK) at 25 °C using disposable square polystyrene cuvettes (for size and PDI) or disposable capillary cells (for zeta potential) (Malvern Instrument, UK). The Z-Average diameter and polydispersity index were measured in water and presented as the average value of three measurements, with 15 runs within each measurement. The zeta potential was also measured in water and presented as the average value of three measurements, with 20-25 runs within each measurement. The mean and standard deviation (SD) of size and zeta potential were calculated for each sample.

2.4 Determination of SPION encapsulation efficiency in *m*-NCs

m-NCs were prepared with increasing loadings of SPIONs (0, 0.38, 1.84 and 7.02 % w/w SPION/NC) and purified by size exclusion chromatography (Sephadex® G-75 column, size exclusion chromatography) to remove any un-encapsulated SPIONs. The Fe content was determined by inductively couple plasma mass spectrometry (ICP-MS, Perkin Elmer SCIEX ICP mass spectrometer, ELAN DRC 6100, USA). For ICP-MS measurements, Fe standards

(Leeman Labs Inc., USA) were prepared in 20 % nitric acid to obtain a standard curve in the range of 10-10000 parts per billion with respect to Fe. *m*-NCs were digested in 2 ml of nitric acid in Falcon™ 15mL conical centrifuge tubes (Fisher Scientific, UK) and incubated overnight at 50 °C. The resulting solution was diluted by 10 times with water before the measurements.

2.5 Determination of DiR encapsulation efficiency in *m*-NCs

The encapsulation efficiency of DiR in *m*-NCs was assessed using a UV/fluorescence spectrometer (Varian, Cary Eclipse, Australia). Prior to quantification, *m*-NC-DiR suspensions were purified by a PD-10 desalting column (size exclusion chromatography) and eluted in PBS buffer to remove any free DiR. The *m*-NC suspensions before and after purification were diluted in DMSO (1/19, v/v) to rupture the NC structure. The excitation/emission wavelengths for the detection of DiR were 740/785 nm. The encapsulation efficiency was expressed as the percentage of the encapsulated dye to the total amount of DiR added to the formulation. All measurements were performed in triplicate and expressed as mean ± SD (n=3).

2.6 Radio-labelling of *m*-NCs and serum stability studies

To radio-label the *m*-NCs with indium-111, *m*-NCs were prepared as described in the previous section except that $PLGA_{18kDa}\text{-}PEG_{3.5kDa}\text{-}DTPA$ was included at 10 % (w/w) of the total polymer content. The *m*-NC suspension (250 µL, 50 mg/mL of polymer) was incubated with 2 M ammonium acetate (one ninth of the reaction volume, pH 5.5), to which 1 MBq of $^{111}InCl_3$ (Mallinckrodt, UK) was added for gamma counting. The reaction was kept at room temperature for 30 min with intermittent vortexing every 10 min. Upon completion, the radio-labelling reaction was quenched by the addition of 0.1 M EDTA chelating solution (one

twentieth of the reaction volume). $^{111}InCl_3$ alone was subjected to the same labelling reaction conditions and used as a control.

The *m*-NC-^{111}In was passed through PD-10 columns before injecting into animals to exchange the ammonium acetate buffer (pH 5.5) with PBS (pH 7.4) and remove free ^{111}In-EDTA. The *m*-NCs-^{111}In (~150 μL per injection dose, 25 mg/mL of polymer) were collected from the column and spotted on instant thin layer chromatography (iTLC) strips which were then developed in 0.1 M ammonium acetate containing 50 mM EDTA as a mobile phase. Strips were allowed to dry before being developed and counted quantitatively using a cyclone phosphor detector (Packard Biosciences, UK) to ensure no free ^{111}In-EDTA present in the injected solution.

2.7 Animal studies and tumor inoculation

All animal experiments were performed in compliance with the UK Home Office (1989) Code of Practice for the Housing and Care of Animals used in Scientific Procedures. CT26 murine colon carcinoma cells (CT26, ATCC®, CRL-2638TM) were cultured in Advanced RPMI (Roswell Park Memorial Institute) 1640 medium supplemented with 1% L-glutamine, 1% penicillin-streptomycin and 10% fetal bovine serum (FBS), in 5 % CO_2 and 95 % air, at 37 °C. The harvested CT26 cells were suspended in PBS solution (pH 7.4). A total of 1×10^6 cells in 20 μL were injected subcutaneously and bifocally at the hind foot of female BALB/c mice aged 4-6 weeks (Harlan, UK). After inoculation, the tumor volume was measured on day 8 and then every other day using a digital caliper and calculated using Equation (1) [2]

Tumor volume (mm^3) = (4/3) * π $(A/2)^2$ *$(B/2)$ =$0.52A^2B$ (1)

where *A* and *B* represent the width and the length of the tumors, respectively. All experiment were carried out (*m*-NCs administration) when the tumor volume reached approximately 500 mm^3.

2.8 Magnetic targeting setup *in vivo*

Disk-shaped nickel-coated neodymium iron boron ($Nd_2Fe_{14}B$) magnets (Magnet Expert Ltd, Tuxford, UK) were used for the *in vivo* magnetic drug targeting studies. That was an 8 mm diameter, 5 mm thick, N42 grade magnet (product code F324), which had a reported field strength of 0.43 Tesla (T) and a reported 'vertical pull' parameter (a measure of the mass of material that the magnet could lift) of 1.9 kg. Single magnet was placed non-invasively over the surface of one of the bifocal tumors and retained using surgical tapes. The contralateral tumor was used as an internal negative control where no magnet was applied. The magnet was then removed at 1 h post-injection of *m*-NCs.

2.9 Fibered confocal fluorescence microscopic imaging studies

The visualization of *m*-NCs in tumor vasculature *in vivo* upon the application of a magnetic field was performed using a fibered confocal fluorescence microscopy (FCFM) imaging system (Cellvizio®, Mauna Kea Technologies, Paris, France). CT26 tumor-bearing BALB/c mice were injected *via* the tail vein with *m*-NC-DiR with a SPION content of 125 mg/kg and DiR content of 9.4 mg/kg (corresponding to 312.5 mg polymer/kg). FITC-Dextran (MW 2,000 kDa, 500 mg/kg, 150 μL) was injected intravenously immediately prior to FCFM imaging to visualize the microvascular network. A small incision (~0.5 cm) was made to insert the laser probe. The exposed tissues were kept moist with PBS pre-warmed to 37 °C. During the time of acquisition, mice were placed in the prone position (tumor and muscle) or supine position (liver) and anesthetized with 1.5 % isoflurane/98.5 % oxygen. Body temperature was controlled by a probe-coupled heating mat. Images and videos were acquired using an S-1500 probe with a penetration depth of 15 µm below tissue surface. To image *m*-NCs in the tumor vasculature upon exposure to a magnetic field in real-time, a set of

magnets (10 disc magnets, 0.43 T, product code F324, Magnet Expert Ltd, Tuxford, UK) was placed adjacent to the surgical incision for 10 min.. FCFM imaging was performed before, during and after application of a magnetic field. Extravasation of the *m*-NCs through blood vessel wall and accumulation over time were also assessed in tumor (TU+ and TU-), quadriceps femoris muscle and liver at 1, 4 and 24 h post-injection. All imaging was carried out using a frame rate of 9 Hz (full FOV), a field of view of 618×609 μm and 100 % laser power at 488 and 660 nm. Images and videos were analyzed using Cellvizio® dual viewer (Mauna Kea Technologies, Paris, France) and videos were reconstructed using ImageJ software.

2.10 Assessment of blood circulation, organ biodistribution and tumor accumulation profiles of *m*-NCs by gamma counting

Blood circulation, organ biodistribution and tumor accumulation profiles of *m*-NC-^{111}In with increasing SPION contents (0, 5, 25 and 125 and 500 mg/kg), representing *m*-NC-5, *m*-NC-25, *m*-NC-125, *m*-NC-500, respectively, were assessed quantitatively in CT26 tumor-bearing BALB/c mice using gamma counting. Mice were injected intravenously *via* tail vein with ~0.7 MBq *m*-NC-[111]In (150 μL in PBS). Magnetic targeting was applied as described in supplementary information. Blood samples (5 μL) were collected from the tail vein at 10 min, 30 min, 1 h, 4 h and 24 h post-injection. Liver, spleen, magnetically-targeted tumors (TU+) and non-magnetically targeted tumors (TU-) were excised and weighed. The radioactivity was measured by a gamma counter (1280 CompuGamma Universal Gamma Counter, LKB Wallac, Finland), using the appropriate energy windows for [111]In. Results were expressed as percentage of injected dose (% ID) in blood or per gram organ or tumor (% ID/g) as means ± SEM (standard error of the mean) (n=3).

2.11 Statistics Statistical Analysis

All statistical tests were performed using IBM SPSS version 20. The significance (p-value) was determined. One-way ANOVA was performed using IBM SPSS Statistics 20 software followed by Tukey's multiple comparison test using Origin 8.6 software. When p-values were 0.05 or less, differences were considered statistically significant.

3. Results and discussion

3.1 Preparation and characterization of magnetic nanocapsules (*m*-NCs)

We designed a magnetic nanocapsule system (*m*-NCs) encapsulating a high amount of superparamagnetic iron oxide nanoparticles (SPIONs) which enables successful magnetic drug targeting *in vivo*. The *m*-NCs were designed in such a way that they can be imaged with optical imaging (due to DiR incorporation), MR imaging (due to SPION) and nuclear imaging (by chelation of radioactive indium-111 (^{111}In) to diethylene triamine pentaacetic acid (DTPA) conjugated to the polymer). These triple-labeled *m*-NCs combined with imaging techniques such SPECT/CT and fibered confocal fluorescence microscopy allowed us to examine the kinetics of *m*-NCs accumulation/extravasation in mice organs, including tumors, on a microscopic scale when an external magnetic field was applied.

PEGylated oil-cored polymeric magnetic nanocapsules (*m*-NCs) were prepared using a single emulsification/solvent evaporation method.[16] *m*-NCs of increasing SPION loadings: 0%, 0.4%, 1.8% and 7% w/w SPION/NC were prepared affording NC, *m*-NC-25, *m*-NC-125 and *m*-NC-500, respectively, were prepared. DiR/SPION encapsulation efficiency (%EE), hydrodynamic sizes (200 to 220 nm) and zeta potentials (- 30 to - 45 mV) are summarized in **Table 1** and **Table 2**.

Table 1. Physicochemical characterization of PEGylated NCs and *m*-NCs prepared by a single emulsification/solvent evaporation method

Formulation[a]	Hydrodynamic size (nm)[b],[e]	PDI [b],[e]	Zeta potential (mV)[c],[e]	DiR EE%[d],[e]
NC	203 ± 4	0.12 ± 0.01	-45 ± 2	-
m-NC	205 ± 3	0.16 ± 0.01	-36 ± 1	-
NC-DiR	206 ± 5	0.16 ±0.01	-39 ± 2	99 ± 4
m-NC-DiR	209 ± 2	0.19 ±0.02	-32 ± 1	95 ± 5

[a] Formulations were prepared with a SPION content of 1.85% w/w SPION/NC
[b] Values were measured with dynamic light scattering and measured in deionized water
[c] Values were obtained with laser Doppler electrophoresis and measured in deionized water
[d] Values were determined by fluorescence spectroscopy
[e] Results are expressed as mean ± SD (n=3)

Table 2. Physicochemical characterization of PEGylated NCs with different SPION loadings prepared by a single emulsification/solvent evaporation method.

Formulation	Hydrodynamic size (nm)[a],[e]	PDI[a], [e]	Zeta potential (mV)[b], [e]	SPION EE%[c], [e]	Initial SPION loading (% w/w, SPION/NC)[d]	Final SPION loading (% w/w, SPION/NC)[d], [e]
NC	203 ± 4	0.12 ± 0.01	-45 ± 2	-	0.00	0.00
m-NC-25	218 ± 4	0.17 ± 0.02	-39 ± 1	99 ± 2	0.38	0.38 ± 0.01
m-NC-125	205 ± 3	0.16 ± 0.01	-36 ± 1	95 ± 3	1.85	1.76 ± 0.06
m-NC-500	214 ± 9	0.19 ± 0.02	-31 ± 1	94 ± 9	7.02	6.60 ± 0.63

[a] Size was measured with dynamic light scattering and measured in deionized water
[b] Values were obtained with laser Doppler electrophoresis and measured in deionized water
[c] Iron content was determined by ICP-MS
[d] Weight of NCs includes polymer, lecithin, castor oil, SPION and tween 80®. Initial and final loading refers to SPION content before and after size exclusion chromatography.
[e] Results are expressed as mean ± SD (n=3)

3.2 The correlation between blood circulation time of *m*-NCs and tumor accumulation under passive and magnetic targeting conditions

We firstly assessed the blood circulation time, reticuloendothelial system (RES) organs, and tumor accumulation of *m*-NCs with an increasing amount of SPIONs *in vivo* in the presence (TU+) or absence (TU-) of a magnetic field in a subcutaneous CT26 (murine colon carcinoma) tumor model. These *m*-NCs were radio-labeled with ^{111}In and their concentrations in blood and tumors were measured by gamma counting. **Figs. 1a** and **b** show the percentage

injection dose (% ID) of *m*-NCs accumulated in the tumor (+/- magnetic field) against the amount remaining in blood at 4 h. Non-magnetic NC, *m*-NC-5, *m*-NC-25, *m*-NC-125 showed comparable blood circulation time with the exception of *m*-NC-500 which exhibited significantly shorter blood circulation time. A linear relationship ($r^2 = 0.8650$) between % ID/g tumor and % ID in blood was shown in the absence of a magnetic field, i.e. TU- (**Fig. 1a**). The good correlation between these two parameters indicates that passive tumor accumulation was dependent on the blood concentration of *m*-NCs, as reported in the literature.[18] On the other hand, this linearity could not be achieved when a magnetic field was applied, i.e. TU+. This suggests that the magnetic force was able to influence the tumor uptake. **Fig. 1c** shows the %ID/g in RES organs, e.g., liver and spleen. The high uptake of *m*-NC-500 in both organs corresponded well to the reduced blood circulation time and contributed to its low TU- accumulation.
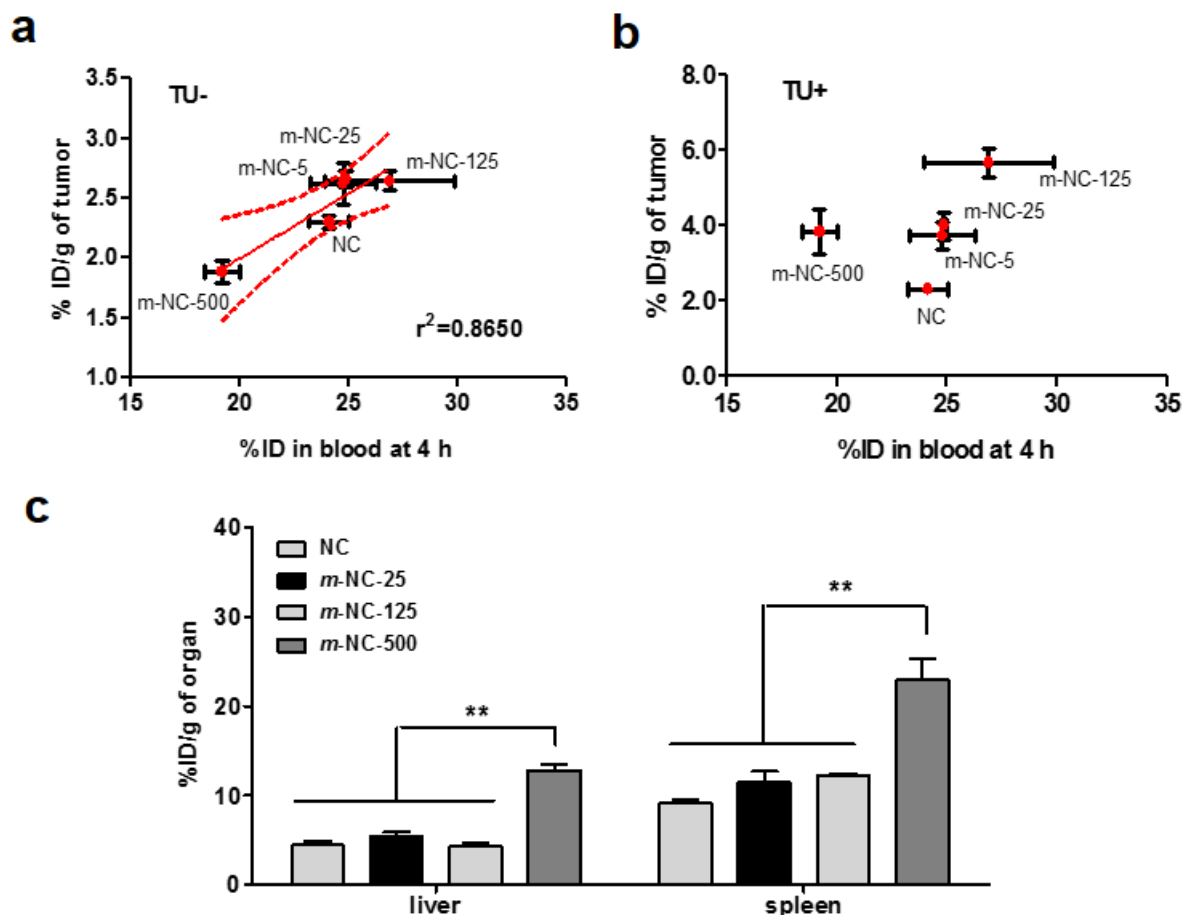
Fig. 1 Organ biodistribution studies of *m*-NC-^{111}In in CT26 tumor-bearing BALB/c mice under the influence of a magnetic field. Mice were intravenously injected with NC-^{111}In or *m*-NC-^{111}In at SPION content of 25, 125 and 500 mg/kg. Blood samples were collected at specified time points and organs and tumors were excised at 24 h post-injection. Scatter plots of %ID of *m*-NCs in tumor tissue (24 h) without (a) or with (b) magnetic targeting as a function of blood concentration (4 h). The best-fit linear regression line along with the 95% confidence band is shown with a correlation coefficient (r^2) of 0.8650 in tumor tissue without magnetic targeting (TU-). (c) Liver and spleen accumulation profiles of m-NC-111In with an increasing amount of SPION. Results are expressed as % ID/g of organ as mean ± SEM (n=3). One-way ANOVA was performed using IBM SPSS version 20 followed by Tukey's multiple comparison test (**$p < 0.01$).

3.3 Live fibered confocal fluorescence microscopic imaging of *m*-NCs in tumor blood vessel under the influence of a magnetic field

The investigation of the effect of magnetic forces on *m*-NC accumulation kinetics in the tumor vasculature is limited by the imaging resolution and invasiveness. As a result, to visualize it dynamically on a microscopic vascular level, a fibered confocal fluorescence

13

microscopy system (FCFM, Cellvizio®, Mauna Kea Technology, Paris, France) was used in this study. Non-magnetic NCs (used as a negative control) and *m*-NCs were fluorescently labeled with DiR as an optical probe. Fluorescein isothiocyanate–dextran (FITC-Dextran), used as a vascular contrast agent, remained in the blood vessels and no leakage up to 1 h has been reported. Mice were inoculated bi-focally with subcutaneous tumors. The imaging probe was inserted into the tumors *via* a small incision and tissues were kept moist throughout the experiment. The imaging protocol is schematically presented in **Fig. 2**. *m*-NCs were injected at 0 h and a magnetic field was then applied to one tumor for 1 h. Multiple imaging was performed at 1,4 and 24 h.
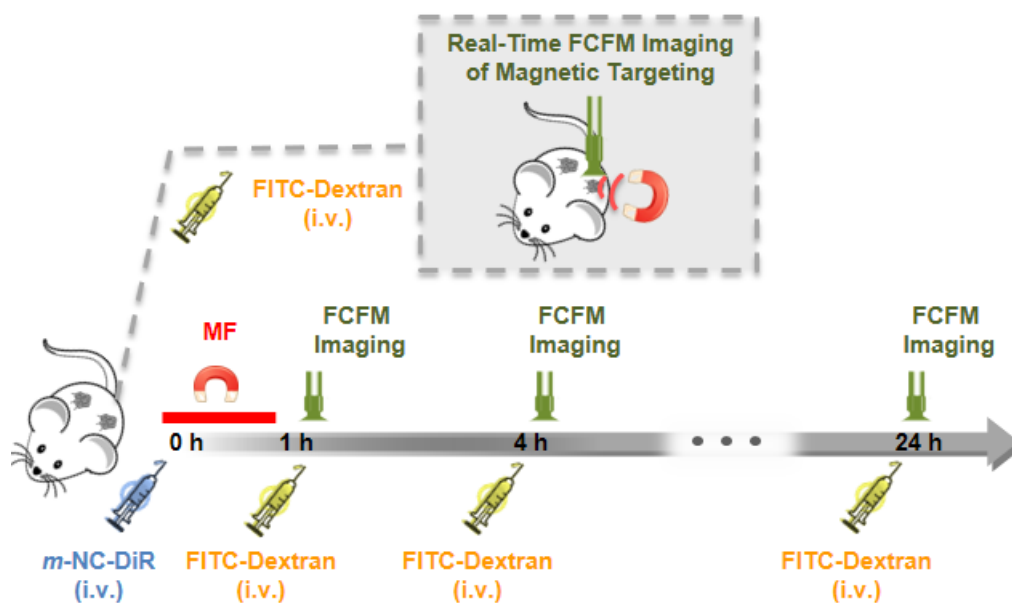

Fig. 2 Experimental timeline of fibered confocal fluorescence microscopic (FCFM) imaging of *m*-NCs in tumor vasculature under the influence of a magnetic field (MF). CT26 tumor-bearing BALB/c mice were injected intravenously with *m*-NC-DiR and a magnet was applied only at one of the bifocal tumors (TU+) for 1 h. FCFM imaging was performed at 1, 4 and 24 h post-injection in both TU+ and TU-. Non-previously injected mouse was used for each time point. FITC-Dextran was injected intravenously at a dose of 500 mg/kg prior to each imaging time point as a macromolecular contrast agent. Inset (top) shows the dynamic FCFM imaging of *m*-NCs in tumor blood vessels during MF application to demonstrate the interaction of *m*-NCs and MF on a microscopic scale.

Prior to application of a magnetic field, DiR-labeled non-magnetic NCs were observed homogenously distributed in blood vessels (**Fig. 3a**, left panel; **Movies 1a-c**). The application of a magnetic field did not cause any changes in the distribution of non-magnetic NCs within the blood vessels. *m*-NCs, on the other hand, behaved differently when a set of magnets was applied in close proximity to the vessels. DiR labeled *m*-NCs started to magnetize, and those magnetized sufficiently appeared as clusters and enriched near the blood vessel wall (**Fig. 3a**, right panel; **Movies 1d-f**). The *m*-NC aggregation was reversible upon removal of the magnetic field due to the superparamagnetism of *m*-NCs.[1, 2, 19] More importantly, the blood vessels appeared intact with no observation of vessel leakage of FITC-Dextran induced by the application of the magnetic field, suggesting no vascular damage *per se*. The enrichment of *m*-NCs within the tumor microvasculature or further enhanced retention in blood vessels would raise the probability of extravasation into the tumor interstitium and thereby increasing tumor uptake.

The *m*-NC distribution in both TU- and TU+ over time was also studied using FCFM. Tumors are heterogeneous and contain irregular capillary networks and non-vascularized areas of necrosis.[20-22] FCFM imaging was performed focusing on the highly vascularized regions. FCFM images showed clear co-localization of FITC-Dextran and *m*-NC-DiR in tumor blood vessels at 1 h and 4 h, confirming the prolonged blood circulation of *m*-NCs (**Fig. 3b**).[16] As expected, DiR signals became more diffuse and spread out throughout the tumor interstitium at 24 h. Interestingly, more intensive signals were seen in TU+ compared to TU-, suggesting enhanced tumor accumulation upon magnetic targeting, consistent with our previously published work.[16]
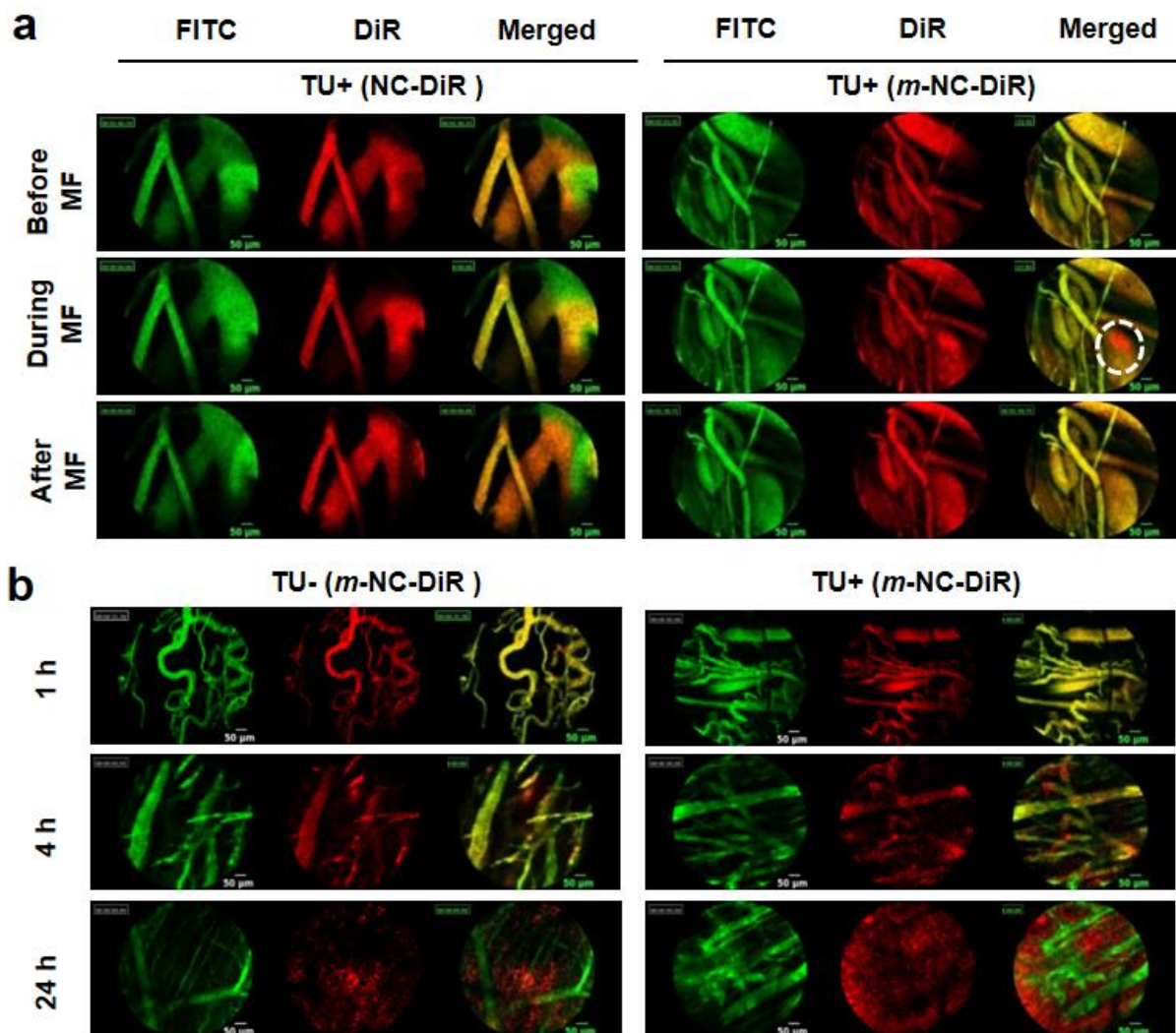
Fig. 3 Live fibered confocal fluorescence microscopic (FCFM) images of *m*-NCs in tumor tissues. *m*-NC-DiR were injected intravenously into CT26 tumor-bearing BALB/c mice and imaged with FCFM using FITC-Dextran as the vascular contrast agent. (a) Real-time FCFM imaging of fluorescently labeled non-magnetic NC (NC-DiR) or magnetic NC (*m*-NC-DiR) (red signals) in tumor blood vessels (green signals) with an external magnetic field (MF) applied at the external part of tumor (TU+), for both formulations. Dashed circle shows the magnetized *m*-NC-DiR, and not NC-DiR is concentrated in the blood vessels upon the application of a magnetic field. (b) Representative single frame FCFM images of *m*-NC-DiR in non-magnetically targeted tumors (TU-) and magnetically targeted tumors (TU+) at 1, 4 and 24 h post-injection. All images were acquired using the Cellvizio® dual band imaging system. Please refer to the videos (supplementary information) for clearer targeting pattern. Scale bar is 50 um.

16

3.4 Real-time fibered confocal fluorescence microscopic imaging of *m*-NCs extravasation in healthy tissues

The extravasation of *m*-NCs were also assessed in healthy tissues to validate the usefulness for real-time nanoparticle imaging. Muscle and liver which exhibit distinct vascular characteristics were used as examples.[23] **Fig. 4** (left panel) shows muscle blood vessels. No DiR signal was visible in the blood vessels of muscle tissues at 24 h, in contrary to the 1 h time point where *m*-NCs were seen in the vasculature. This is consistent with *m*-NC distribution data, where no *m*-NC retention was seen in muscle at 24 h, due to the continuous capillaries and complete basement membrane.[16, 24, 25] It was also confirmed that DiR labeling was confined to the *m*-NCs and the dye did not translocate to cellular membrane. In contrast, a number of *m*-NCs leaked out of the liver sinusoids and accumulated in non-vascular liver tissues at 24 h (**Fig. 4**, right panel), consistent with gradual liver accumulation over time described in our previously published work.[16] This was not surprising as the liver vasculature has an incomplete basement membrane and transcytoplasmic openings.[25]
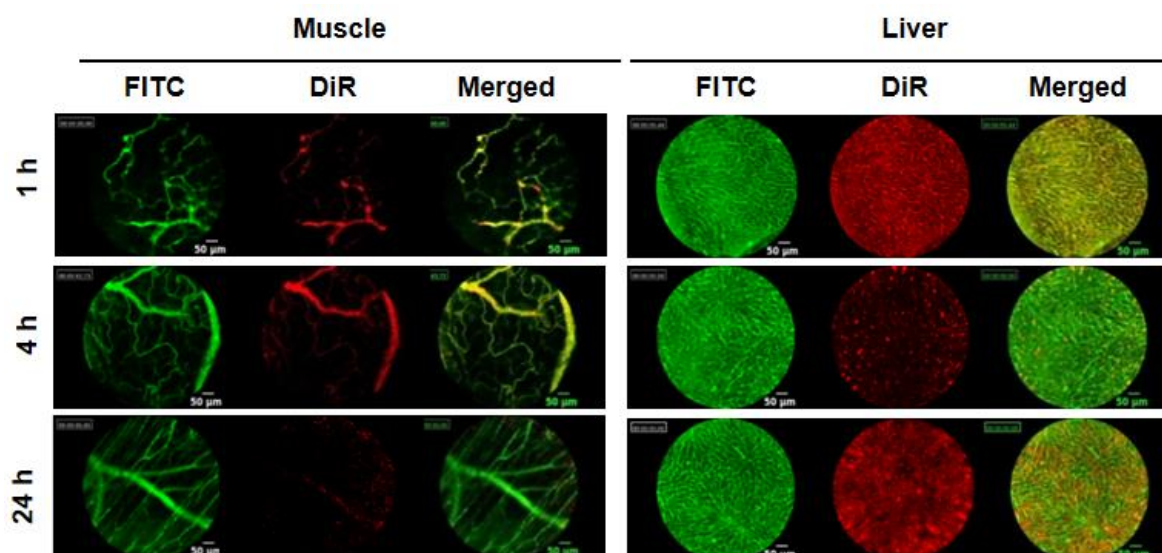
Fig. 4 Real-time fibered confocal fluorescence microscopic (FCFM) images of *m*-NCs in muscle and liver. *m*-NC-DiR were injected intravenously into CT26 tumor-bearing BALB/c mice and imaged with FCFM using FITC-Dextran as the vascular contrast agent. Representative single frame FCFM images of *m*-NC in muscle and liver tissues at 1, 4 and 24 h post-injection with the application of a magnetic field at the tumor. All images were acquired using the Cellvizio® dual band imaging system. Scale bar is 50 um.

It is conceivable from experimental physics and prior knowledge that magnetic nanoparticles (MNPs) can be attracted by the magnetic forces in tumour blood vessel and be concentrated to the tumour tissue. A number of studies indeed have demonstrated that MNPs could be concentrated in the tumour under the influence of a magnetic field by MRI [5, 11]. However, MRI cannot provide sufficient resolution to image the MNP in tumour vasculature. Whether or not the magnetic forces acting on individual *m*-NC is strong enough to overcome blood flow has not been addressed. A direct visualisation in a time-course study is required.

The FCFM provides real-time *in vivo* microvascular observations and *in situ* high spatial resolution imaging (up to 1.4 μm) at vascular level. It also represents a significant advantage over traditional intra-vital microscopic imaging (IVM) which usually requires invasive surgical procedures and is limited by the availability of animal models that bear visually accessible tumours in a dorsal skinfold chamber. FCFM enables micro-invasiveness and

requires only a small incision at the imaging site. Small openings can be sutured if the animals are required to be kept for long-term studies.

4. Conclusion

A number of studies have explored magnetic targeting in drug delivery. However, this is the first report of real-time live imaging of magnetic targeting in tumor vasculature on the microscopic scale. The novel application of FCFM described in this study offers direct visualisation of *m*-NCs within blood vessels and in tumour tissues before, during and after magnetic field exposure in a real-time manner, with high resolution and minimal surgical intervention. Our results suggested that the distribution of *m*-NCs within tumour vasculature changed dramatically, but in a reversible way, upon application and removal of a magnetic field. The *m*-NCs were concentrated and stayed as clusters near a blood vessel wall when tumours were exposed to a magnetic field but without rupturing the blood vessel. This work bridges the gap between previous findings of enhanced tumor uptake with magnetic targeting and the nanocarrier behavior at the blood-tumor vasculature-tumor tissue interface, thanks to the high resolution characteristics of this imaging modality. This proof-of-concept descriptive study in mice is envisaged to track and quantify nanoparticles *in vivo* in a non-invasive manner with microscopic resolution.
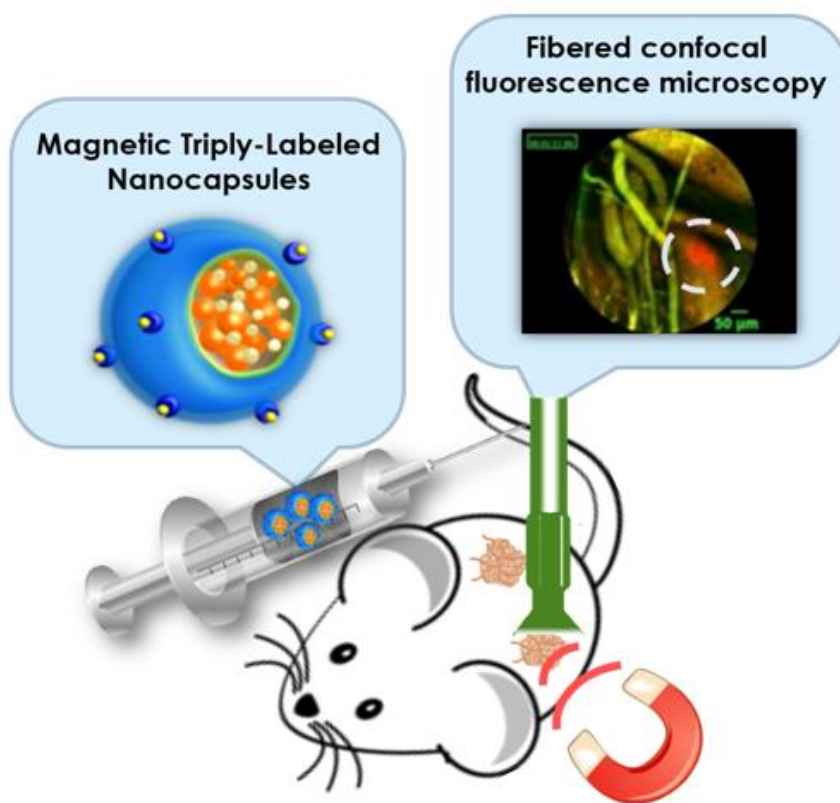
19

References

[1] Q.A. Pankhurst, J. Connolly, S. Jones, J. Dobson, Applications of magnetic nanoparticles in biomedicine, J Phys D: Appl Phys, 36 (2003) R167.

[2] M. Arruebo, R. Fernández-Pacheco, M.R. Ibarra, J. Santamaría, Magnetic nanoparticles for drug delivery, Nano Today, 2 (2007) 22-32.

[3] R. Jurgons, C. Seliger, A. Hilpert, L. Trahms, S. Odenbach, C. Alexiou, Drug loaded magnetic nanoparticles for cancer therapy, J. Phys.: Condens. Matter, 18 (2006) S2893.

[4] B. Chertok, A.E. David, V.C. Yang, Brain tumor targeting of magnetic nanoparticles for potential drug delivery: effect of administration route and magnetic field topography, J Control Release, 155 (2011) 393-399.

[5] B. Chertok, B.A. Moffat, A.E. David, F. Yu, C. Bergemann, B.D. Ross, V.C. Yang, Iron oxide nanoparticles as a drug delivery vehicle for MRI monitored magnetic targeting of brain tumors, Biomaterials, 29 (2008) 487-496.

[6] C. Alexiou, R. Tietze, E. Schreiber, R. Jurgons, H. Richter, L. Trahms, H. Rahn, S. Odenbach, S. Lyer, Cancer therapy with drug loaded magnetic nanoparticles — magnetic drug targeting J Magn Magn Mater, 323 (2011) 1404-1407.

[7] C. Alexiou, R. Jurgons, R.J. Schmid, C. Bergemann, J. Henke, W. Erhard, E. Huenges, F. Parak, Magnetic drug targeting-biodistribution of the magnetic carrier and the chemotherapeutic agent mitoxantrone after locoregional cancer treatment, J Drug Target, 11 (2003) 139-149.

[8] S.H. Hu, T.Y. Hsieh, C.S. Chiang, P.J. Chen, Y.Y. Chen, T.L. Chiu, S.Y. Chen, Surfactant‐free, lipo‐polymersomes stabilized by iron oxide nanoparticles/polymer interlayer for synergistically targeted and magnetically guided gene delivery, Adv Healthc Mater, (2013).

[9] B. Chertok, A.E. David, Y. Huang, V.C. Yang, Glioma selectivity of magnetically targeted nanoparticles: a role of bbnormal tumor hydrodynamics, J Control Release, 122 (2007) 315-323.

[10] L. Zhang, F. Yu, A.J. Cole, B. Chertok, A.E. David, J. Wang, V.C. Yang, Gum arabic-coated magnetic nanoparticles for potential application in simultaneous magnetic targeting and tumor imaging, AAPS J. , 11 (2009) 693-699.

[11] A.S. Lübbe, C. Bergemann, H. Riess, F. Schriever, P. Reichardt, K. Possinger, M. Matthias, B. Dörken, F. Herrmann, R. Gürtler, Clinical experiences with magnetic drug targeting: a phase I study with 4′-Epidoxorubicin in 14 patients with advanced solid tumors, Cancer Res, 56 (1996) 4686-4693.

[12] A. Nacev, C. Beni, O. Bruno, B. Shapiro, The behaviors of ferromagnetic nano-particles in and around blood vessels under applied magnetic fields, J Magn Magn Mater, 323 (2011) 651-668.

[13] A. Nacev, C. Beni, O. Bruno, B. Shapiro, Magnetic nanoparticle transport within flowing blood and into surrounding tissue, Nanomedicine (Lond), 5 (2010) 1459-1466.

[14] R. Tietze, H. Rahn, S. Lyer, E. Schreiber, J. Mann, S. Odenbach, C. Alexiou, Visualization of superparamagnetic nanoparticles in vascular tissue using XμCT and histology, Histochem Cell Biol, 135 (2011) 153-158.

[15] S. Lyer, R. Tietze, R. Jurgons, H. Richter, F. Wiekhorst, K. Schwarz, L. Trahms, C. Alexiou, Distribution of magnetic manoparticles after magnetic drug targeting in an rx vivo bovine artery model, in: Histochem Cell Biol, Springer, 2009, pp. 484-487.

[16] J. Bai, J.T.-W. Wang, N. Rubio, A. Protti, H. Heidari, R. Elgogary, P. Southern, W.T. Al-Jamal, J. Sosabowski, A.M. Shah, Triple-modal imaging of magnetically-targeted nanocapsules in solid tumours in vivo, Theranostics, 6 (2016) 15.

[17] R.I. El-Gogary, N. Rubio Carrero, J.T.-W. Wang, W.T. Al-Jamal, M. Bourgognon, H. Kafa, M. Naeem, R. Klippstein, V. Abbate, F. Leroux, Polyethylene glycol conjugated polymeric nanocapsules for targeted delivery of quercetin to folate-expressing cancer cells in vitro and in vivo, ACS Nano, (2014).

[18] S. Nie, Understanding and overcoming major barriers in cancer nanomedicine, Nanomedicine (Lond), 5 (2010) 523.

[19] M. Chorny, I. Fishbein, S. Forbes, I. Alferiev, Magnetic nanoparticles for targeted vascular delivery, IUBMB life, 63 (2011) 613-620.

[20] N. Faye, L. Fournier, D. Balvay, F. Taillieu, C. Cuenod, N. Siauve, O. Clement, Dynamic contrast enhanced optical imaging of capillary leakage, Technol Cancer Res Treat, 10 (2011) 49-57.

[21] A. Pierucci, P. Teixeira, V. Zimmermann, F. Sirveaux, M. Rios, J.-L. Verhaegue, A. Blum, Tumours and pseudotumours of the soft tissue in adults: Perspectives and current role of sonography, Diagn Interv Imaging, 94 (2013) 238-254.

[22] H. Hashizume, P. Baluk, S. Morikawa, J.W. McLean, G. Thurston, S. Roberge, R.K. Jain, D.M. McDonald, Openings between defective endothelial cells explain tumor vessel leakiness, Am J Pathol, 156 (2000) 1363-1380.

[23] M. Derieppe, A. Yudina, M. Lepetit-Coiffé, B.D. De Senneville, C. Bos, C. Moonen, Real-time assessment of ultrasound-mediated drug delivery using fibered confocal fluorescence microscopy, Mol Imaging Biol, 15 (2013) 3-11.

[24] L.R. Johnson, Essential medical physiology, Academic Press, 2003.

[25] G.E. Palade, Fine structure of blood capillaries, J Appl phys, 24 (1953) 1424-1436.

Graphical abstract